



## Hadron and Electron Response of Uranium/Liquid Argon Calorimeter Modules for the D0 Detector\*

*The D0 Calorimeter Group*

M. Abolins<sup>10</sup>, S.-C. Ahn<sup>14</sup>, S. H. Aronson<sup>1</sup>, R. Astur<sup>10</sup>, J. F. Bartlett<sup>5</sup>, G. C. Blazey<sup>13</sup>, J. Borders<sup>13</sup>, A. D. Bross<sup>5</sup>, J. H. Christenson<sup>5</sup>, W. E. Cooper<sup>5</sup>, D. Cutts<sup>2</sup>, M. Demarteau<sup>14</sup>, P. Draper<sup>13</sup>, S. Durston<sup>13</sup>, D. Edmunds<sup>10</sup>, J. Featherly<sup>1</sup>, T. Ferbel<sup>13</sup>, H. E. Fisk<sup>5</sup>, G. E. Forden<sup>14</sup>, P. Franzini<sup>4</sup>, B. G. Gibbard<sup>1</sup>, J. Gerecht<sup>12</sup>, M. L. Good<sup>14</sup>, H. A. Gordon<sup>1</sup>, P. D. Grannis<sup>14</sup>, J. A. Guida<sup>14</sup>, J. M. Guida<sup>1</sup>, W. Guryn<sup>1</sup>, N. J. Hadley<sup>15†</sup>, H. Haggerty<sup>5</sup>, S. Hagopian<sup>7</sup>, T. Heuring<sup>14</sup>, R. Hirosky<sup>13</sup>, J. S. Hoftun<sup>2</sup>, A. S. Ito<sup>5</sup>, M. E. Johnson<sup>5</sup>, A. M. Jonckheere<sup>5</sup>, S. Kahn<sup>1</sup>, D. Kewley<sup>13</sup>, C. Klopfenstein<sup>9‡</sup>, W. Kononenko<sup>12</sup>, J. Kotcher<sup>11</sup>, J. Kourlas<sup>11</sup>, S. Libonate<sup>13</sup>, J. T. Linnemann<sup>10</sup>, S. Linn<sup>7</sup>, F. Lobkowicz<sup>13</sup>, R. J. Madras<sup>9</sup>, H. J. Martin<sup>8</sup>, M. Marx<sup>14</sup>, R. McCarthy<sup>14</sup>, K. W. Merritt<sup>5</sup>, P. Mooney<sup>10</sup>, P. Nemethy<sup>11</sup>, D. Nešić<sup>11</sup>, K. K. Ng<sup>14</sup>, D. P. Owen<sup>10</sup>, M. Paterno<sup>14</sup>, B. Pi<sup>10</sup>, H. Piekarz<sup>7</sup>, B. G. Pope<sup>10</sup>, S. Protopopescu<sup>1</sup>, R. Raja<sup>5</sup>, K. Roberts<sup>3</sup>, R. D. Schamberger<sup>14</sup>, J. Sculli<sup>11</sup>, W. Selove<sup>12</sup>, R. P. Smith<sup>5</sup>, A. L. Spadafora<sup>9</sup>, M. L. Stevenson<sup>9</sup>, M. Timko<sup>14§</sup>, E. Treadwell<sup>5</sup>, P. M. Tuts<sup>4</sup>, H. D. Wahl<sup>7</sup>, H. Wang<sup>12</sup>, H. Weerts<sup>10</sup>, W. A. Wenzel<sup>9</sup>, A. P. White<sup>6</sup>, S. J. Wimpenny<sup>3</sup>, W. J. Womersley<sup>6</sup>, P. Yamin<sup>1</sup>, S. Youssef<sup>7</sup>, and A. Zieminski<sup>8</sup>

• <sup>1</sup> Brookhaven National Laboratory, Upton, New York 11973 • <sup>2</sup> Brown University, Providence, Rhode Island 02912 •

<sup>3</sup> University of California, Riverside, California 92521 • <sup>4</sup> Columbia University, New York, New York 10027 •

<sup>5</sup> Fermi National Accelerator Laboratory, Batavia, Illinois 60510 • <sup>6</sup> University of Florida, Gainesville, Florida 32611 •

<sup>7</sup> Florida State University, Tallahassee, Florida 32306 • <sup>8</sup> Indiana University, Bloomington, Indiana 47401 •

<sup>9</sup> Lawrence Berkeley Laboratory, Berkeley, California 94720 • <sup>10</sup> Michigan State University, East Lansing, Michigan 48824 •

<sup>11</sup> New York University, New York, New York 10003 • <sup>12</sup> University of Pennsylvania, Philadelphia, Pennsylvania 19104 •

<sup>13</sup> University of Rochester, Rochester, New York 14627 • <sup>14</sup> State University of New York, Stony Brook, New York 11794 •

<sup>15</sup> Yale University, New Haven, Connecticut 06511 •

February 1989

\* To be published in Nucl. Instrum. Methods A



Operated by Universities Research Association, Inc., under contract with the United States Department of Energy

# Hadron and Electron Response of Uranium / Liquid Argon Calorimeter Modules for the D0 Detector

The D0 Calorimeter Group

M. Abolins<sup>10</sup>, S.-C. Ahn<sup>14</sup>, S. H. Aronson<sup>1</sup>, R. Astur<sup>10</sup>, J. F. Bartlett<sup>5</sup>, G. C. Blazey<sup>13</sup>, J. Borders<sup>13</sup>, A. D. Bross<sup>5</sup>, J. H. Christenson<sup>5</sup>, W. E. Cooper<sup>5</sup>, D. Cutts<sup>2</sup>, M. Demarteau<sup>14</sup>, P. Draper<sup>13</sup>, S. Durston<sup>13</sup>, D. Edmunds<sup>10</sup>, J. Featherly<sup>1</sup>, T. Ferbel<sup>13</sup>, H. E. Fisk<sup>5</sup>, G. E. Forden<sup>14</sup>, P. Franzini<sup>4</sup>, B. G. Gibbard<sup>1</sup>, J. Gerecht<sup>12</sup>, M. L. Good<sup>14</sup>, H. A. Gordon<sup>1</sup>, P. D. Grannis<sup>14</sup>, J. A. Guida<sup>14</sup>, J. M. Guida<sup>1</sup>, W. Guryn<sup>1</sup>, N. J. Hadley<sup>15†</sup>, H. Haggerty<sup>5</sup>, S. Hagopian<sup>7</sup>, T. Heuring<sup>14</sup>, R. Hirosky<sup>13</sup>, J. S. Hoftun<sup>2</sup>, A. S. Ito<sup>5</sup>, M. E. Johnson<sup>5</sup>, A. M. Jonckheere<sup>5</sup>, S. Kahn<sup>1</sup>, D. Kewley<sup>13</sup>, C. Klopfenstein<sup>9†</sup>, W. Kononenko<sup>12</sup>, J. Kotcher<sup>11</sup>, J. Kourlas<sup>11</sup>, S. Libonate<sup>13</sup>, J. T. Linnemann<sup>10</sup>, S. Linn<sup>7</sup>, F. Lobkowicz<sup>13</sup>, R. J. Madaras<sup>9</sup>, H. J. Martin<sup>8</sup>, M. Marx<sup>14</sup>, R. McCarthy<sup>14</sup>, K. W. Merritt<sup>5</sup>, P. Mooney<sup>10</sup>, P. Nemethy<sup>11</sup>, D. Nešić<sup>11</sup>, K. K. Ng<sup>14</sup>, D. P. Owen<sup>10</sup>, M. Paterno<sup>14</sup>, B. Pi<sup>10</sup>, H. Piekarczyk<sup>7</sup>, B. G. Pope<sup>10</sup>, S. Protopopescu<sup>1</sup>, R. Raja<sup>5</sup>, K. Roberts<sup>3</sup>, R. D. Schamberger<sup>14</sup>, J. Sculli<sup>11</sup>, W. Selove<sup>12</sup>, R. P. Smith<sup>5</sup>, A. L. Spadafora<sup>9</sup>, M. L. Stevenson<sup>9</sup>, M. Timko<sup>14§</sup>, E. Treadwell<sup>5</sup>, P. M. Tuts<sup>4</sup>, H. D. Wahl<sup>7</sup>, H. Wang<sup>12</sup>, H. Weerts<sup>10</sup>, W. A. Wenzel<sup>9</sup>, A. P. White<sup>6</sup>, S. J. Wimpenny<sup>3</sup>, W. J. Womersley<sup>6</sup>, P. Yamin<sup>1</sup>, S. Youssef<sup>7</sup>, and A. Zieminski<sup>8</sup>.

<sup>1</sup> Brookhaven National Laboratory, Upton, NY 11973

<sup>2</sup> Brown University, Providence, RI 02912

<sup>3</sup> University of California, Riverside, CA 92521

<sup>4</sup> Columbia University, New York, NY 10027

<sup>5</sup> Fermi National Accelerator Laboratory, Batavia IL 60510

<sup>6</sup> University of Florida, Gainesville, FL 32611

<sup>7</sup> Florida State University, Tallahassee, FL 32306

<sup>8</sup> Indiana University, Bloomington, IN 47401

<sup>9</sup> Lawrence Berkeley Laboratory, Berkeley, CA 94720

<sup>10</sup> Michigan State University, East Lansing, MI 48824

<sup>11</sup> New York University, New York, NY 10003

<sup>12</sup> University of Pennsylvania, Philadelphia, PA 19104

<sup>13</sup> University of Rochester, Rochester, NY 14627

<sup>14</sup> State University of New York, Stony Brook, NY 11794

<sup>15</sup> Yale University, New Haven, CT 06511.

† Present address: University of Maryland, College Park, MD 20742

‡ Present address: CEN-Saclay, 91191 Gif-sur-Yvette, France

§ Present address: Texas A & M University, College Station, TX 77843

## Abstract

We present the results of tests made on two types of uranium/liquid argon calorimeter modules, one electromagnetic and one hadronic, constructed for the D0 detector at the Fermilab Tevatron Collider. For electrons and hadrons with energies between 10 and 150 GeV, we present measurements of energy resolution, linearity of response, electromagnetic to hadronic response ratio ( $e/\pi$ ), and longitudinal hadronic shower development. We have also investigated the effects of adding small amounts of methane to the liquid argon.

### 1. Introduction

The D0 detector is presently under construction and will study proton-antiproton collisions at 1.8 TeV at the Fermilab Tevatron. One of the salient features of the detector is its calorimetry which is intended to provide good energy resolution for jets and electrons as well as good shower containment. To meet these objectives, and for compactness, radiation hardness and uniformity of response, uranium-liquid argon was chosen for the calorimetry. A previous study<sup>[1]</sup> verified the choice of design and explored various options for the geometry. The purpose of the present tests was to confirm that full prototypes of D0 calorimeter modules would perform as expected by exploring their response to electrons and pions over a range of energies. The results of adding methane to the liquid argon were also investigated. The modules used were electromagnetic sections of the central calorimeter and a middle hadronic section of the end calorimeter. The locations of these modules in the full detector are indicated in Fig. 1.

### 2. Calorimeter Test Set-up

The tests were carried out in the NW beam at Fermilab. The beam energies used were 10, 25, 50, 75, 100 and 150 GeV for both electrons and pions (the beam polarity was negative, so the hadron beam was mainly pions and will be referred to as such). The beam was operated in slow spill mode over a 20 second time interval, with the instantaneous rate limited to about 1500 particles per second to reduce pileup. The beam had a momentum spread of 1.0% and a physical spot size at the modules of about 40 mm diameter. The beamline was instrumented with scintillator counters to form the trigger, and with proportional wire counters with 1 mm wire spacing for the reconstruction of beam particle momentum and track position.

The central calorimeter electromagnetic (CCEM) modules contain 21 radiation lengths (0.76 interaction lengths) of material\* in the form of a stack of 20 uranium plates 3 mm thick, 2.60 m long and with widths varying from 160 to 200 mm, separated from each other by 5.7 mm, as shown in Fig. 2. The uranium absorber plates are grounded. A G-10 signal board is placed in the center of the gap between absorber plates to collect the charge. On the liquid argon side the boards are covered with a layer of resistive epoxy maintained at negative high voltage. Signals are read out from pads machined on a copper plane on the inside of the board. Thus the G-10 insulator forms an integral blocking capacitor. The pads sum the signal from both argon gaps. The pad size in D0 is such as to form towers with intervals of pseudorapidity and azimuth of  $\Delta\eta \times \Delta\phi = 0.1 \times 0.1$  as viewed from the D0 interaction point. The pad sizes thus vary with position in the module; the front pads in the middle are about  $40 \times 40$  mm. The CCEM modules are read out in 4 layers (respectively 2, 2, 7, 10 radiation lengths deep). The third layer, which sees the peak of the shower, has smaller pads ( $\Delta\eta \times \Delta\phi = 0.05 \times 0.05$ ) for better position resolution. In these tests, the modules were positioned in an open stainless steel vessel filled with liquid argon inside a cryostat. The vessel contained 5 CCEM modules, 2 in front and 3 behind, oriented so that the beam entered through the front face, as shown in Fig. 3(a).

The end calorimeter middle hadronic (ECMH) module contains 8.1 interaction lengths of material and is approximately 1.5 m long and 0.6 m  $\times$  0.7 m in cross section (in fact, it forms a truncated  $22.5^\circ$  wedge of one of the annular sections of the end calorimeter). It consists of a uranium-liquid argon stack, containing 4.0 interaction lengths, followed by a steel-liquid argon leakage section. The uranium section uses 6 mm plates of uranium-niobium(2%) alloy. The readout gaps are similar to the ones in the CCEM modules. All readout pad sizes are as needed to form  $\Delta\eta \times \Delta\phi = 0.1 \times 0.1$  towers, corresponding to pad areas of about 150 mm  $\times$  150 mm. The towers are projective as viewed from the D0 interaction point, leading to their axes being inclined at about  $30^\circ$  relative to the long dimension of the module. The uranium section is longitudinally segmented into four layers (each having 15 readout gaps). The steel section, forming one longitudinal readout layer, uses 46.5 mm thick stainless steel plates in place of the uranium plates with the gap and board geometry kept the same. The beam entered normal to the front face of the module, *i.e.* perpendicular to all the argon gaps, as shown in Fig. 3(b).

---

\* We have used radiation length and nuclear interaction length values as quoted by the Particle Data Group<sup>[2]</sup>.

Twisted pair cables within the cryostat were used to carry the signals from a given readout depth in the module to a multilayer feedthrough board. This board brought the signals out of the cryostat and mapped them so that all the signals in a particular tower became adjacent. Short cables connected the external side of the feedthrough to hybrid preamplifiers located on the side of the cryostat. The output of the preamps was connected by twisted pair cables to a rack of hybrid base line subtractors (BLS). The BLS's shaped the signal and sampled it twice with an interval of  $2.5 \mu\text{s}$ . The difference of the two samples was buffered and transported via 6 twisted pair cables to analog to digital converters (ADC). The signals from the BLS's were time multiplexed so that one ADC read out 384 BLS channels. The ADC's had 12 bit precision, but the use of a switchable  $\times 1/ \times 8$  amplifier enabled 15 bit dynamic range to be achieved. The ADC's resided in a VME crate and were read out by the standard D0 data acquisition system: data flowed over 40 MB/s cable directly from VME into a dual port memory channel in a selected event filtering node, one of a "farm" of three MicroVAX-II computers. The sensitivity of this digitization system is such that one ADC count was equivalent to 3500 electrons (for the  $\times 8$  gain setting). The readout was triggered by a simple coincidence of the scintillator counters in the beam.

### 3. Data Analysis

The data were taken between September 1987 and February 1988. There were three periods of data-taking with CCEM modules (a total of 9 different modules), and two with the ECMH module, during this time.

The data were analyzed off-line using the following procedure. ADC pedestals were determined for each channel using pulser-triggered pedestal runs taken between data runs. The pedestal runs also provided a way of verifying that there were no dead or disconnected channels. The pedestal counts were subtracted from the ADC counts obtained for each channel in each data event. The experiment was also equipped with a pulser system capable of injecting a fixed charge through a precision resistor into each preamp channel for the determination of the relative gains. The rms spread in relative gains was 2.3 %; the correction was not used in the analysis presented here.

In the analysis of CCEM data only the towers immediately adjacent to the shower maximum were added to calculate the incident energy (for a total of 9 towers), while for the ECMH data signals from all 112 towers were added.

In the analysis of ECMH data, the energy from the coarse section at the rear of the stack was weighted by the ratio of sampling fractions for this section relative to the uranium section to yield a uniform response per unit deposited energy. The sampling fraction was defined as:

$$SF = t_{Ar} \frac{dE}{dx_{Ar}} \bigg/ \left( t_{Ar} \frac{dE}{dx_{Ar}} + t_{G-10} \frac{dE}{dx_{G-10}} + t_{Absorber} \frac{dE}{dx_{Absorber}} \right) \quad (1)$$

where  $dE/dx$  is the mean energy lost by a minimum ionizing particle in each type of material (taken from Ref. [2]) and  $t$  is the thickness of each material in any cell of the readout tower. The sampling fractions thus determined are 6.75% for the uranium section and 1.64% for the steel section.

Cuts were made on the data to remove events with more than one track in the beam wire chambers upstream of the calorimeter, and events where the peak energy deposition was far from the expected beam position.

#### 4. High Voltage Behavior

The data presented here suffer from two problems that will not affect the final D0 calorimeters. One difficulty was the presence of discharges within the calorimeter cells. These caused pulses at the preamp outputs which were added in with beam-associated energy deposition. The discharge pulses had a slow rise time (5–10  $\mu$ s) compared with signal pulses ( $\sim 2\mu$ s), and an amplitude spectrum approximately  $\sim 1/(\text{amplitude})^{1/2}$ . The rate of discharging increased over about one day after high voltage was applied and then declined slowly with a time constant of 4–20 days\*. The discharge rates through the runs were tracked using an oscilloscope, and also through off-line studies of pedestal runs where the discharge rate was monitored by counting the number of pedestals beyond 3 standard deviations from the mean. Thus we were able to select data from periods when the discharges had reached as low a rate as possible.

A second difficulty was that the response of the module to the beam of a fixed energy was observed to decay over a period of a few days: approximately 10% of the signal was

---

\* This discharge phenomenon has been shown in subsequent tests to be dependent on the presence of uranium absorber plates, resistive coated signal boards and negative high voltage. For the final D0 calorimeters, the problem is avoided by using positive high voltage on the signal boards.

lost over two weeks. The most likely explanation for this was that the liquid argon in the calorimeter became contaminated with oxygen entering through known leaks in the cryostat. A liquid argon test cell has subsequently been used to measure the amount of oxygen in the liquid argon and a rate of contamination of about 0.2ppm/day was seen. Studies on the effects and sources of oxygen contamination are continuing. In this analysis, data taken more than about a day apart in time have not been compared because of this loss of signal.

Figure 4 shows the high voltage plateau obtained for one CCEM and the ECMH module using 50 GeV pions, together with those of some other liquid argon detectors: Fermilab experiment 706<sup>[3]</sup> (lead absorber), CERN experiment NA34<sup>[4]</sup> (uranium absorber) and the D0 test beam results from 1985<sup>[1]</sup> (uranium absorber). The curves for the CCEM and ECMH modules are seen to be similar to those of the other detectors. The operating voltage used for the modules was 2.5 kV, corresponding to an electric field in the argon of 1.1 kV/mm.

## 5. Response as a Function of Energy

### 5.1 CCEM Modules

Energy scans of the CCEM modules with electron beams were taken at various times. In Figure 5(a) we show a typical ADC count spectrum for 50 GeV electrons. Gaussian fits to the ADC count distribution were used to determine the mean response  $\mu$  (in ADC counts) and resolution  $\sigma$ . We made a linear fit to  $\mu$  for two different CCEM modules. The results of the fits over the energies 10, 25, 50, 75, 100, and 150 GeV are given below:

$$\begin{aligned} \text{module 1} & : \mu = (-337 \pm 6) + (322.9 \pm 0.2)E \\ \text{module 2} & : \mu = (-232 \pm 8) + (322.7 \pm 0.2)E \end{aligned} \tag{2}$$

where E is in GeV. We have corrected for the energy loss in the cryostat, liquid argon vessel walls, inactive argon before the module, and the outer skin of the modules, based on Monte Carlo calculations. These corrections, which range from 250 MeV at 10 GeV to 3 GeV at 150 GeV, do not affect the fit significantly. The response of the two modules is very similar and they track each other as a function of time (the difference in response with time is due to argon contamination as discussed earlier). Deviations from linearity are typically less than 1%, as shown in Fig. 6(a).

The intercepts of the fits are significantly different from zero. We have been unable to find a reason for this. It could be due to an offset in the beam momentum settings but we have not been able to test this possibility.

The response of module 1 to non-interacting particles (assumed to be mainly muons) of 50 GeV is shown in Fig. 5(b). The most probable signal is  $76 \pm 4$  ADC counts for a total sensitive thickness of 94.5 mm of liquid argon.

## 5.2 ECMH Module

Typical spectra of ADC counts for 50 GeV pions, 50 GeV electrons and 150 GeV non-interacting particles in the ECMH module are given in Fig. 5(c), (d) and (e). The difference in response from the CCEM modules is due to the different sampling fraction. The most probable response for 150 GeV non-interacting particles is  $264 \pm 41$  ADC counts, for 325 mm of liquid argon.

Straight line fits to the mean response in ADC counts from 10 to 150 GeV are given below:

$$\begin{aligned} \pi : \mu &= (-209 \pm 17) + (154.7 \pm 0.4)E \\ e : \mu &= (-245 \pm 22) + (161.8 \pm 0.9)E \end{aligned} \tag{3}$$

Figure 6(b) shows deviations of the data from linearity. For the ECMH module these are all less than  $\pm 2\%$ . The CCEM and ECMH modules therefore both show good linearity for electrons and pions above 10 GeV.

## 6. Resolution as a Function of Energy

The fractional resolution ( $\sigma/\mu$ ) is taken from a Gaussian fit to the distribution of (ADC counts)/(beam energy) in the calorimeter. The beam energy is determined event-by-event using the proportional wire counters in the beamline. This removes the effect of the spread in beam energy ( $\sim 1\%$ ) from the resolution. For the CCEM modules, the effects of gain variation between channels were removed by assigning a weight to each channel and fitting the weights to minimize the resolution. The CCEM resolutions were averaged over CCEM modules 1 and 2.

We assume the following energy dependence for the resolution:

$$\left(\frac{\sigma}{\mu}\right)^2 = C^2 + \frac{S^2}{E} + \frac{N^2}{E^2}, \tag{4}$$

where  $E$  is the beam energy in GeV,  $S$  is due to statistical errors in sampling,  $C$  is a constant term reflecting such effects as momentum spread of the beam, upstream energy losses and shower leakage, and non-equal response to electromagnetic and hadronic energy, and  $N$  accounts for energy-independent contributions to  $\sigma$  such as electronic and uranium noise, and discharges. We derived the noise terms  $N$  independently using pedestal runs. This was done by analyzing the pedestal run as though it were data taken at  $E = 0$ : Eqn. 4 shows that as  $E = \mu \rightarrow 0$ ,  $\sigma \rightarrow N$ . The values obtained for  $N$  this way are 140 MeV for CCEM, 1.22 GeV for electrons and 1.28 GeV for pions in the ECMH module. The electron and pion numbers for the ECMH differ, though the noise in ADC counts is independent of particle type, because as shown by equation (3) there is a difference in response of the module to electrons and pions in terms of energy per ADC count. The ECMH numbers are higher than for the CCEM because of the larger pad size, and because the discharge rate in this module was higher. With values of  $N$  as given above, we fit  $(\sigma/\mu)^2$  as a function of  $E$  to obtain the “sampling” and “constant” terms of the resolution  $S$  and  $C$ . Figure 7 shows the values of  $\sigma/\mu$  plotted as a function of  $E$ , together with the results of the fits, for electrons in CCEM module 1 (10–150 GeV) and for electrons and pions in the ECMH module (25–150 GeV). To obtain a good  $\chi^2$  for the fits it was necessary to add a systematic error (of between 5% and 10% of the resolution, depending on module type) in quadrature with the statistical errors on each resolution point. The results of the fits are:

$$\begin{aligned}
\text{CCEM } e : \quad S &= 0.162 \pm 0.011, \quad C = 0.003 \pm 0.004, \quad (N = 0.140); \\
\text{ECMH } e : \quad S &= 0.233 \pm 0.010, \quad C = 0.010 \pm 0.004, \quad (N = 1.22); \\
\text{ECMH } \pi : \quad S &= 0.439 \pm 0.042, \quad C = 0.047 \pm 0.005, \quad (N = 1.28).
\end{aligned}
\tag{5}$$

If alternatively  $(\sigma/\mu)^2$  is fit as a function of energy to obtain  $S$ ,  $C$  and  $N$  without constraining  $N$  to the values obtained from the pedestal runs, the values obtained are entirely consistent with those given above, but are less well-determined.

The value of  $S$  obtained for electrons in the ECMH is larger than that for the CCEM because of the coarser sampling (6 mm rather than 3 mm uranium plates). An EGS simulation of electron showers in the ECMH module predicted the resolution at 50 GeV, with no noise contribution, to be 3.5%; equation (5) yields 3.44%, in excellent agreement.

We have attempted to correct the resolution for pions in the ECMH for the effects of shower leakage from the calorimeter, and spread in preamplifier gains. The effect of

shower leakage on resolution is to increase the constant term  $C$  and decrease the sampling term  $S$ . After correcting we estimate the intrinsic performance of the ECMH module to be  $S \sim 0.49 \pm 0.04$  and  $C \sim 0.02 \pm 0.01$ . Shower leakage appears responsible for a large part of the rather large value of  $C$  shown in equation (5). This will not apply in the completed D0 calorimeter where the ECMH will be surrounded with other similar modules.

## 7. Longitudinal Shower Development in the ECMH Module

Given the longitudinal segmentation of this calorimeter module (approximately 1, 1, 1, 1, and 4 interaction lengths per layer) we have investigated the longitudinal development of hadron showers. Figure 8 shows the average energy detected in the calorimeter as a function of the number of interaction lengths traversed, for hadron showers at energies from 25 to 150 GeV. The figure also shows the predictions of the parametrization of Bock et al.<sup>[5]</sup> and measurements from the 1985 D0 tests<sup>[1]</sup>. Our results have been normalized so that they are fixed to agree with the parametrization at the back of the module. The parametrization has been calculated for the geometry and properties of the present module, using an exponential distribution of vertex positions but with no shower fluctuations included. It will be seen that there is reasonably good agreement between the results of this experiment and the parametrization.

## 8. Compensation: $e/\pi$ response

Because of large fluctuations in the electromagnetic component of hadronic showers, hadronic calorimeter resolution improves dramatically if the calorimeter is “compensating”, *i.e.* if the response to electrons and hadrons of a given energy is the same. Wigmans<sup>[6]</sup> has investigated the theory of compensation in some detail.

Our ECMH calorimeter module was exposed directly to pion and electron beams to determine the ratio of respective responses ( $e/\pi$ ) at various energies. Figure 9 shows the values of  $e/\pi$  obtained, with their errors, as a function of energy. The raw response to electrons and pions was corrected for a series of effects listed in table 1 and described below.

- Electron showering in the dead material (scintillators, cryostat, argon vessel, uninstrumented argon and steel front plate) upstream of the first sensitive argon gap of the module. This material amounts to 3.2 radiation lengths (0.37 interaction lengths).

**Table 1**  
Corrections used in evaluating  $e/\pi$

Beam energy (GeV)	10	25	50	75	100	150
$e$ loss upstream(%)	8.8	5.1	3.3	2.6	2.1	1.6
$\pi$ loss upstream (%)	4.1	2.1	1.4	1.2	1.0	0.7
$\pi$ loss transverse (%)	0.6	0.8	1.1	1.2	1.3	1.6
$\pi$ loss downstream (%)	0.4	0.9	1.3	1.6	1.7	2.1
$\pi$ loss total (%)	5.0	3.7	3.8	4.0	4.0	4.4
Correction to $e/\pi$	1.035	1.015	0.995	0.985	0.981	0.971
Systematic error (%)	1.6	1.5	1.7	1.9	2.0	2.3

The energy loss was estimated using the parametrization of Bock *et al.*<sup>[5]</sup> and checked for consistency with EGS at 50 GeV.

- Pion energy loss in the same dead material. Most pions pass through this material without interacting but those that do shower can deposit considerable energy. The mean energy was estimated using the Bock parametrization<sup>[5]</sup> and ranges from 4.1% of the incident energy at 10 GeV to 0.7% at 150 GeV.
- Leakage of hadron energy from the sides and back of the calorimeter. Losses from the sides were estimated using results on transverse shower containment from CDHS<sup>[7]</sup> and Fermilab experiment 733<sup>[8]</sup> and range from a 0.6% loss at 10 GeV to a 1.6% loss at 150 GeV. Losses from the back were estimated using the Bock parametrization<sup>[5]</sup> and range from 0.4% at 10 GeV to 2.1% at 150 GeV.

The errors include a statistical contribution of 0.007 estimated from the spread of the four data runs at 50 GeV (the only energy where more than one measurement was made), and a systematic contribution. The latter includes estimates of the errors on the various energy loss corrections listed above (0.010–0.018); variation in preamp response (0.01, from summing typically five channels with a spread of 2.3%), and uncertainty in the sampling fraction in the steel section compared to the uranium section (0.002–0.004). The corrected data points lie between 1.002 and 1.082, and their mean is  $1.029 \pm 0.008^*$ .

---

\* Our previously obtained value of  $e/\pi$  between 1.11 and 1.13<sup>[1]</sup> had not been corrected for hadron shower leakage.

Figure 9 also shows a predicted curve based on the calculations of Wigmans<sup>[6]</sup>. This curve is derived for an “intrinsic”  $e/h$  of 1.08, as predicted for this detector geometry. The intrinsic  $e/h$  is the ratio of the calorimeter sensitivity to purely electromagnetic and purely hadronic shower components. The measured  $e/\pi$  is closer to unity than  $e/h$  since some fraction  $f_{EM}$  of the hadronic shower energy is electromagnetic in character ( $\pi^0$  production, *etc.*). The energy dependence of this fraction leads to the energy dependence of the predicted  $e/\pi$  curve; following Ref. [6], we assumed an energy dependence of  $f_{EM} = 0.1 \ln E$  (GeV). The prediction is in reasonably good agreement with the measured data points.

### 9. Effect of Adding Methane

Recent studies<sup>[6]</sup> of the part played by slow neutrons in the development of hadronic showers have led to suggestions that calorimeter resolution may be improved, and  $e/\pi$  brought closer to unity, through the introduction of hydrogenous material into the sensitive layers of the calorimeter. This is because the neutron energy can then be converted efficiently to ionization through scattering from protons; the neutron energy is then sampled more effectively and the calorimeter is less influenced by its fluctuations. This effect has been verified in scintillator-readout calorimeters; it might be applied to liquid argon devices through the addition of methane to the liquid argon. This provides a faster collection time in liquid argon at the expense of a somewhat reduced signal. Although it appears plausible that methane would act to improve calorimeter resolution through “conversion” of slow neutrons, calculations<sup>[9]</sup> suggest that an enhancement of saturation effects in the liquid argon when methane is added would outweigh the gain from neutron conversion; this would lead to worsened resolution and  $e/\pi$  deviating away from unity.

In order to investigate the effects of methane on resolution and on  $e/\pi$ , tests were conducted with the ECMH module, using 50 GeV incident pions and electrons for molar concentrations of methane in the liquid argon of 0, 0.5, 1 and 2%.

The effects of adding methane, as illustrated in Fig. 10, are as follows:

- (i) As expected, the response is sharply reduced with increasing amounts of methane. After adding 1%  $\text{CH}_4$  (molar) the signal decreased by 25–30%. Addition of more methane continues to diminish the signal, though at a reduced rate.

- (ii) The resolution for both pions and electrons remains roughly constant with addition of methane.
- (iii) The ratio of responses,  $e/\pi$ , deviates away from unity as methane concentration is increased. The effect is roughly linear from  $e/\pi$  measured to be 1.019 just before the addition of methane to 1.064 with 2% added. This is broadly consistent with Wigmans' prediction<sup>[9]</sup> of a 10% increase in  $e/\pi$  for 2.5% CH<sub>4</sub>.

The addition of small amounts of methane to the liquid argon, therefore, does not have any beneficial effect on the calorimeter resolution and worsens the  $e/\pi$  response.

As a consistency check, we have calculated the expected effect of the change in  $e/\pi$  on the pion resolution of the calorimeter. Using the observed change in electron resolution we estimate a small decrease in noise apparently resulting from the addition of methane. This is combined with the expected effect on resolution of the worsened value of  $e/\pi$ , using Ref. [6], to yield the expected pion resolution with methane. This is in good agreement with the measured resolution.

## Acknowledgments

We are grateful for the support from the Accelerator and Research Divisions at Fermilab, especially the technical staffs under the direction of Delmar Miller and Tom Topolski. We thank Dr. W. Willis of CERN for the loan of part of the cryostat. We thank Dr. D.F. Anderson for his continued interest in these measurements and in particular for his help in the addition of methane. We thank the U.S. Department of Energy and the National Science Foundation for funding this work.

## References

- [1] S. H. Aronson *et al.*, Hadron and electron response in a uranium liquid argon calorimeter from 10–150 GeV, *Nucl. Instr. & Meth.* **A269** (1988) 492.
- [2] Particle Data Group (M. Aguilar-Benitez *et al.*), Review of Particle Properties, *Phys. Lett.* **170B** (1986).
- [3] F. Lobkowicz, private communication, October 1988.
- [4] V. Polychronakos, private communication, December 1988.
- [5] R.K. Bock, T. Hansl-Kozanecka, and T.P. Shah, Parametrization of the Longitudinal Development of Hadronic Showers in Sampling Calorimeters, *Nucl. Instr. & Meth.* **186** (1981) 533.  
  
The parametrization has been evaluated using computer code supplied by T. Hansl-Kozanecka.
- [6] R. Wigmans, On the Energy Resolution of Uranium and Other Hadron Calorimeters, *Nucl. Instr. & Meth.* **A259** (1987) 389.  
  
R. Wigmans, High Resolution Hadron Calorimetry, *Nucl. Instr. & Meth.* **A265** (1988) 273.
- [7] E. Hughes, Measurement of Hadronic and Electromagnetic Shower Development between 10 GeV and 140 GeV by an Iron-Scintillator Calorimeter, CDHS internal report, 1986 (unpublished).
- [8] W.J. Womersley *et al.*, Hadron Showers in a Low-Density Fine-Grained Flash Chamber Calorimeter, *Nucl. Instr. & Meth.* **A267** (1988) 49.
- [9] R. Wigmans, private communication, November 1988.

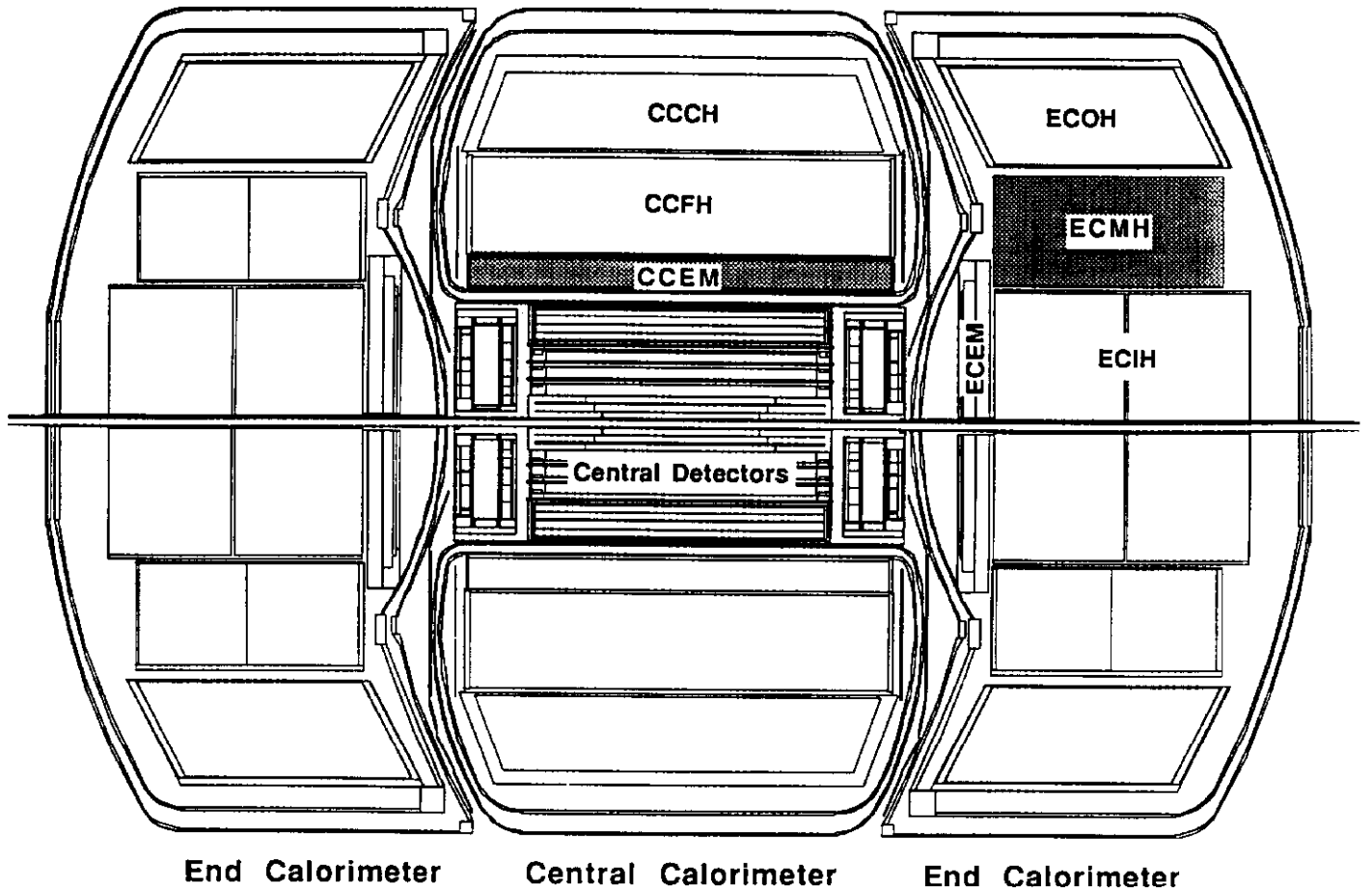


**Figure 1**

Longitudinal section through the calorimeter of the D0 detector for the Fermilab Tevatron collider. The shaded areas show the CCEM and ECMH calorimeter modules used in the present tests.

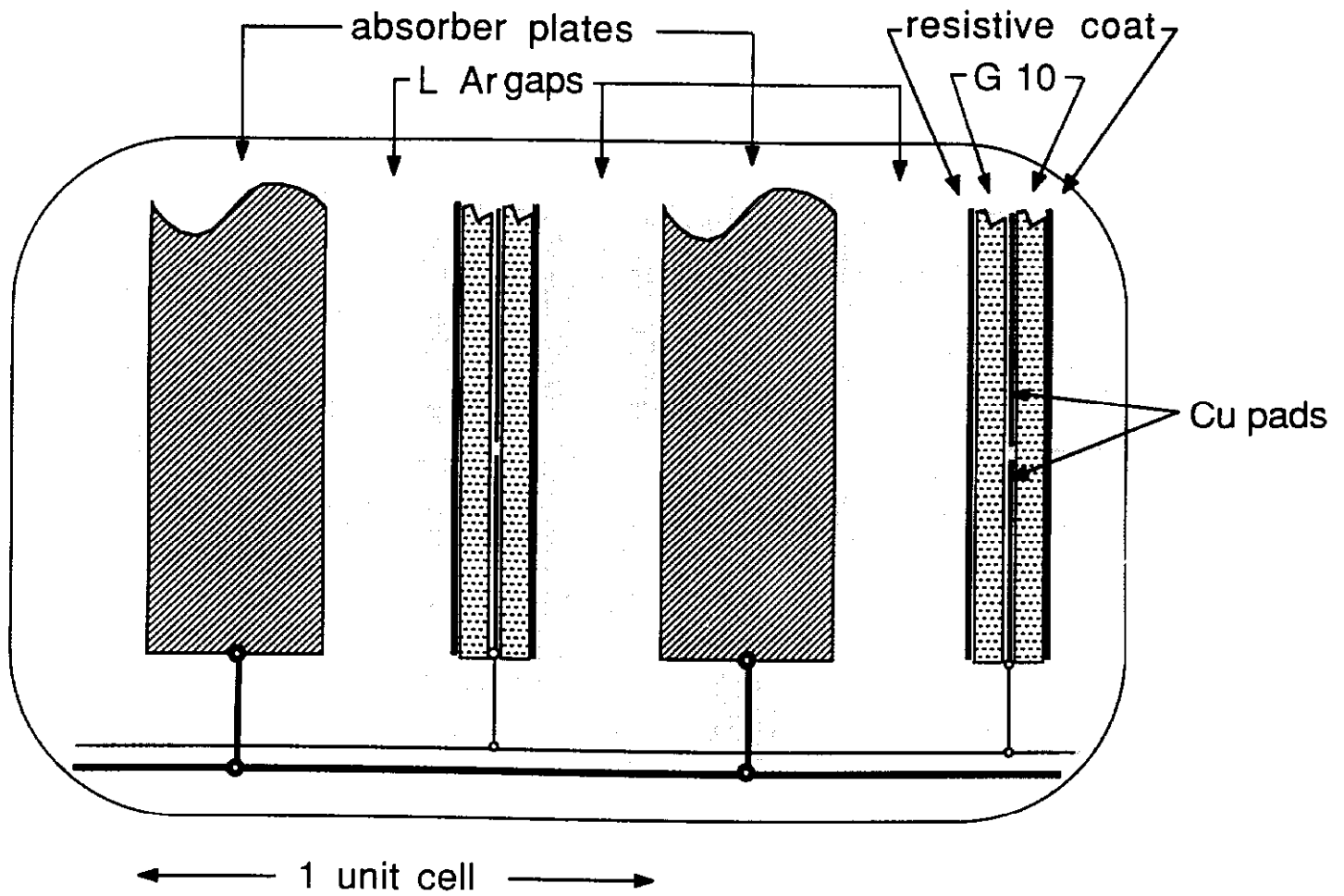


**Figure 2**

Section through part of a calorimeter module, showing the arrangement of absorber plates, liquid argon and signal boards (not to scale).

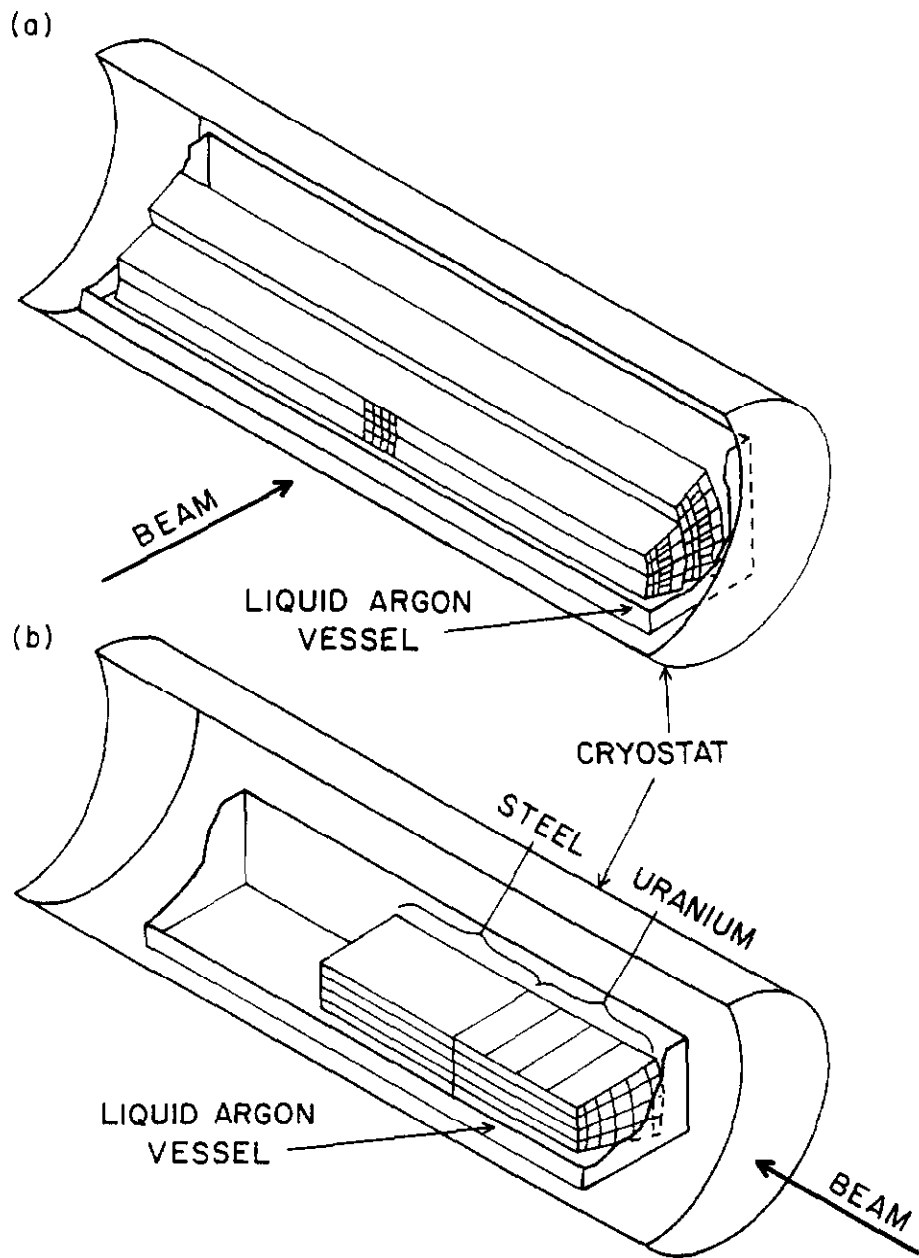


**Figure 3**

Arrangement of modules in the test beam, showing orientation of modules within the cryostat, for (a) CCEM load and (b) ECMH load.

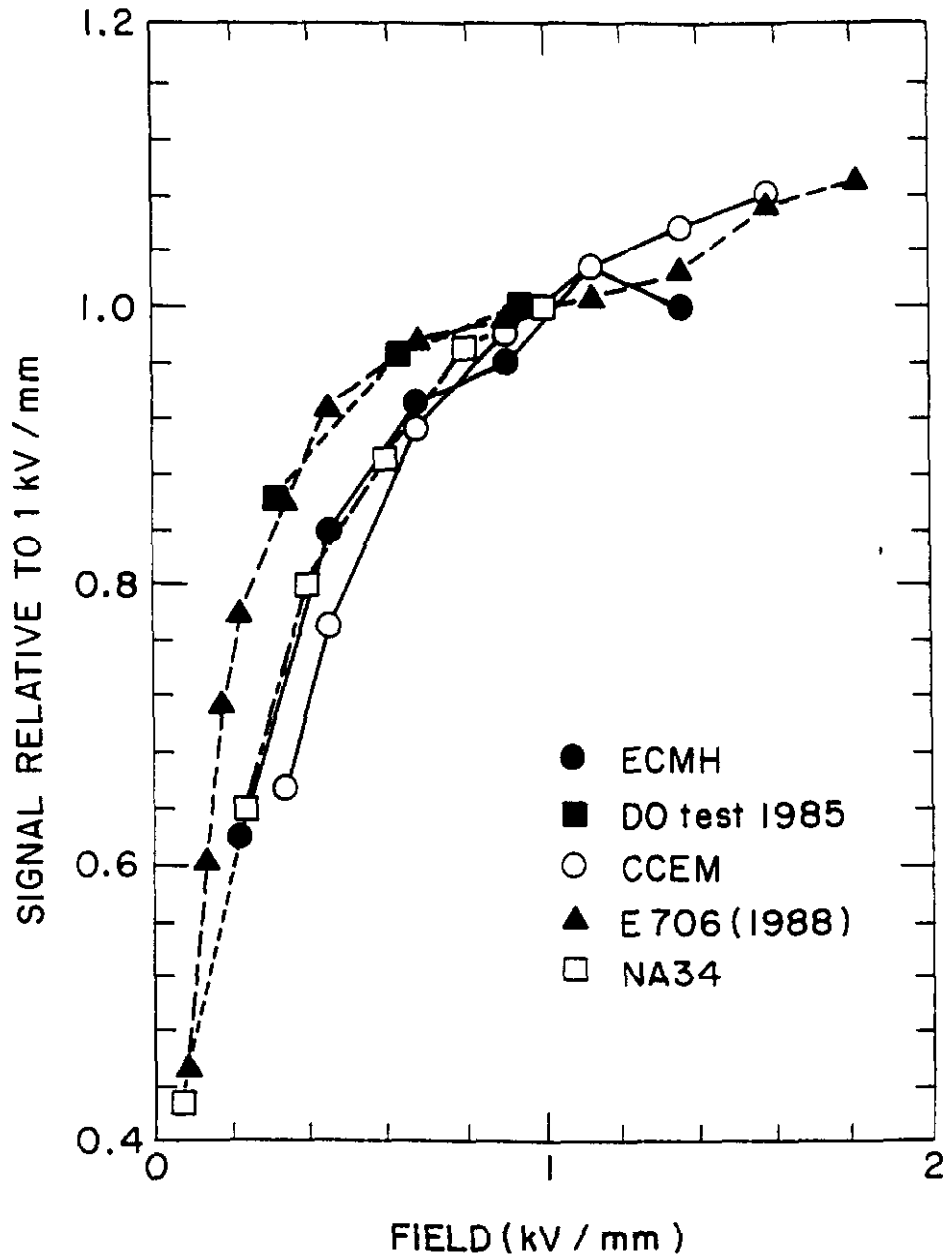


**Figure 4**

Comparison of high voltage plateau curve for one CCEM module (50 GeV electrons), the ECMH module (50 GeV pions), and those of the 1985 D0 test calorimeter (Ref. [1]), Fermilab experiment 706 (Ref. [3]), and CERN experiment NA34 (Ref. [4]). The curves are normalized to unity at 1kV/mm.

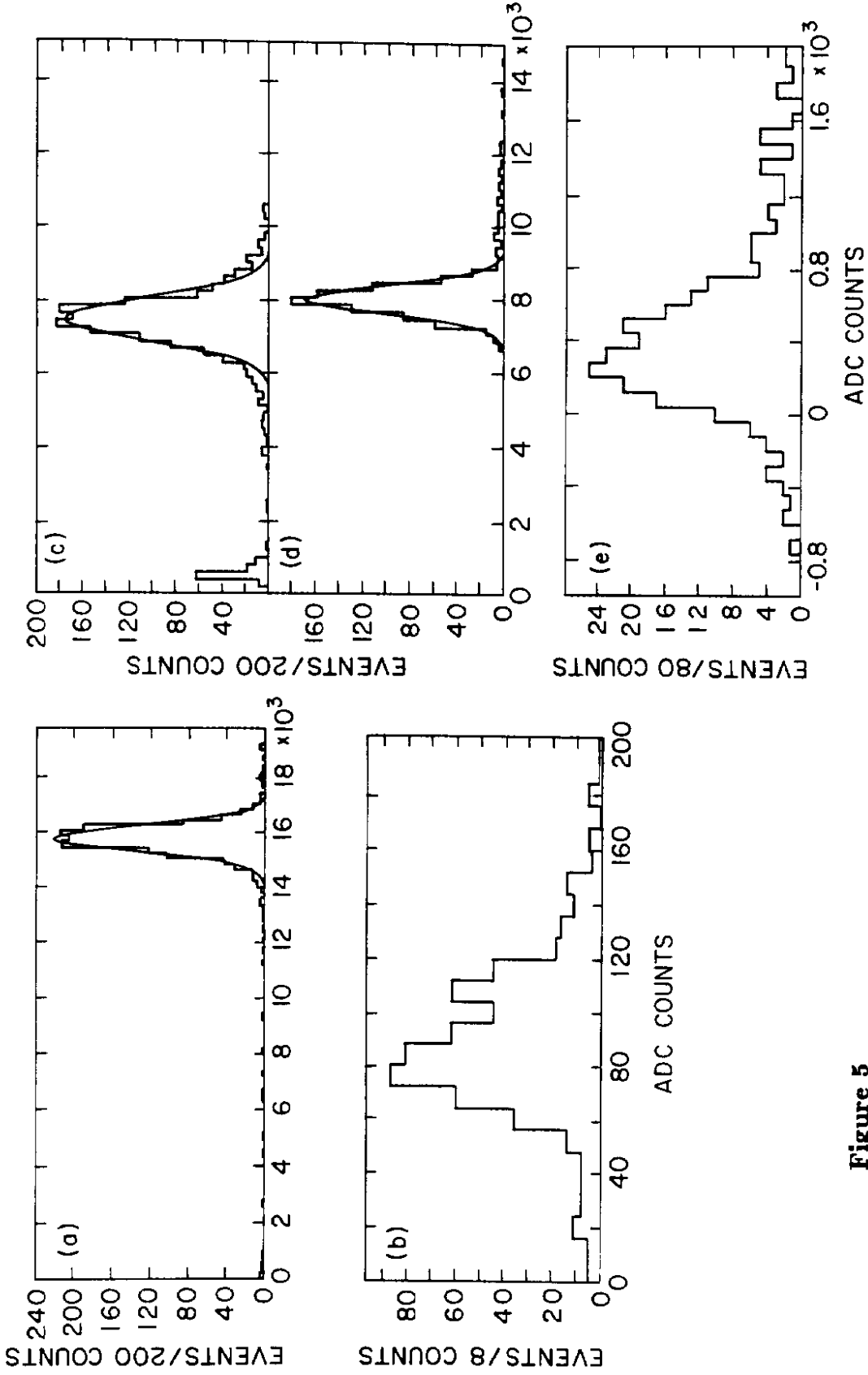


**Figure 5**

Typical ADC count spectra for (a) 50 GeV electrons in the CCEM modules, (b) 50 GeV non-interacting particles in the CCEM, (c) 50 GeV pions in the ECMH, (d) 50 GeV electrons in the ECMH, and (e) 150 GeV non-interacting particles in the ECMH module.

Gaussian fits are shown for (a), (c) and (d). Note the different horizontal scales.

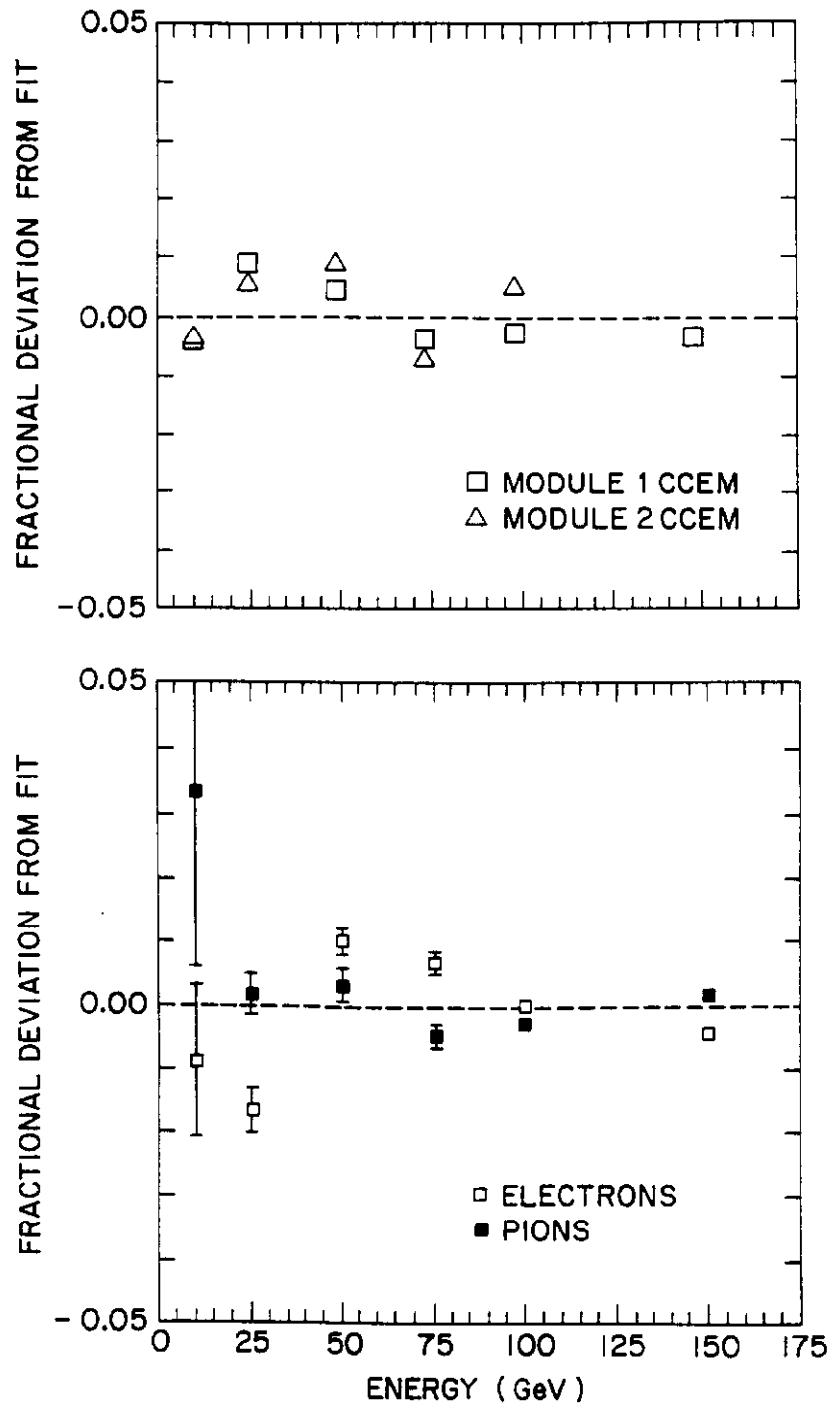


**Figure 6**

Fractional differences between measured response and linearity for (a) CCEM modules (electrons) and (b) ECMH module (electrons and pions).

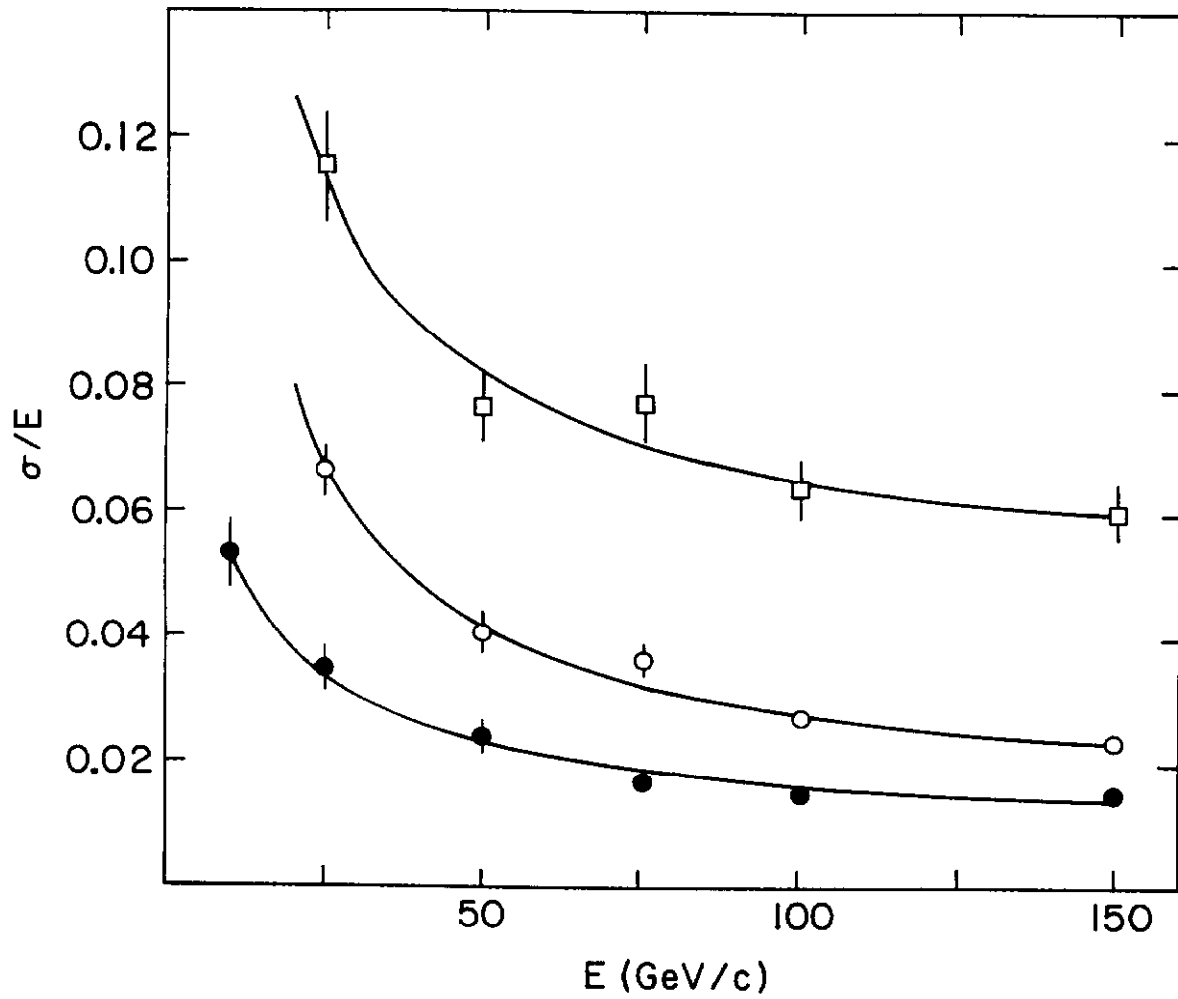


**Figure 7**

Hadron and electron fractional resolution  $\sigma/\mu$  as a function of  $E$ . Solid circles are electrons in the CCEM modules; open circles electrons in the ECMH module, and open squares pions in the ECMH module. The lines show the fits described in the text.

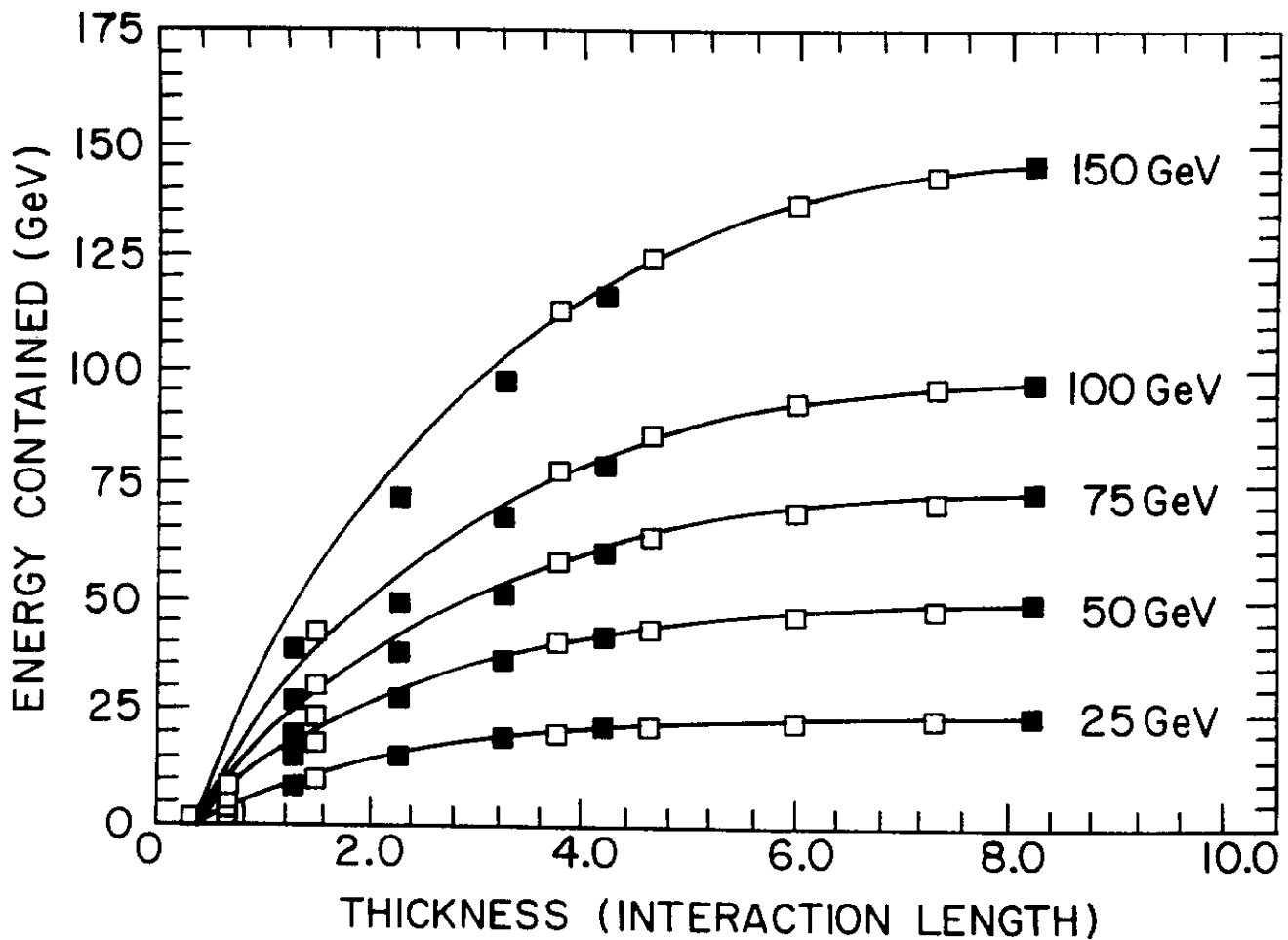


**Figure 8**

Longitudinal shower containment as a function of the number of interaction lengths traversed by the shower.

The curves are the predictions of the parametrization of Bock et al. (Ref. [5]). The solid data points are from this experiment, using pions from the December ECMH run, and have been normalized to agree with the parametrization at the back of the module. The open data points are from the 1985 D0 tests (Ref. [1]).

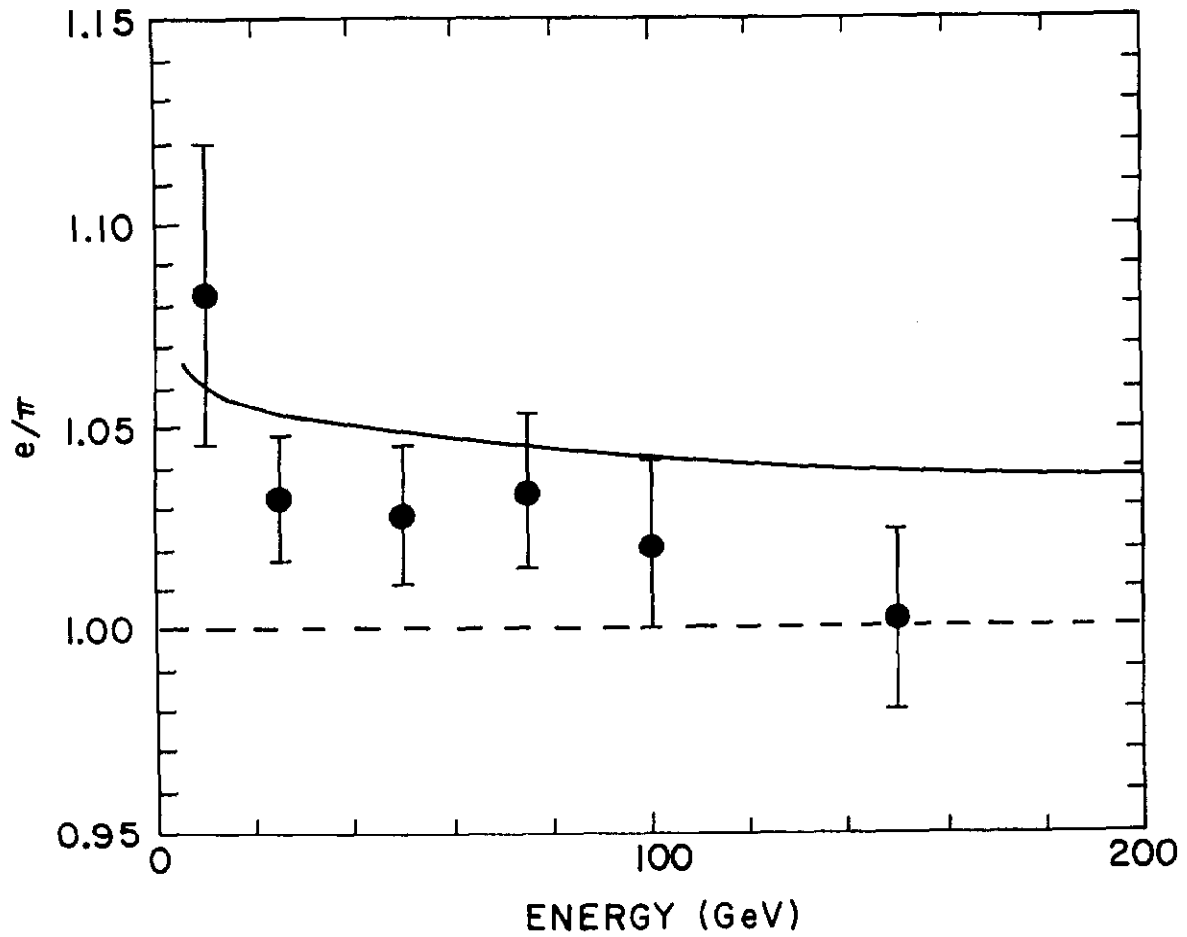


**Figure 9**

Corrected ratios of response,  $e/\pi$ , for various beam energies in the ECMH module. The errors on the data points are systematic and statistical combined. The curve shows the predicted  $e/\pi$  based on the calculations of Wigmans (Ref. [6]).

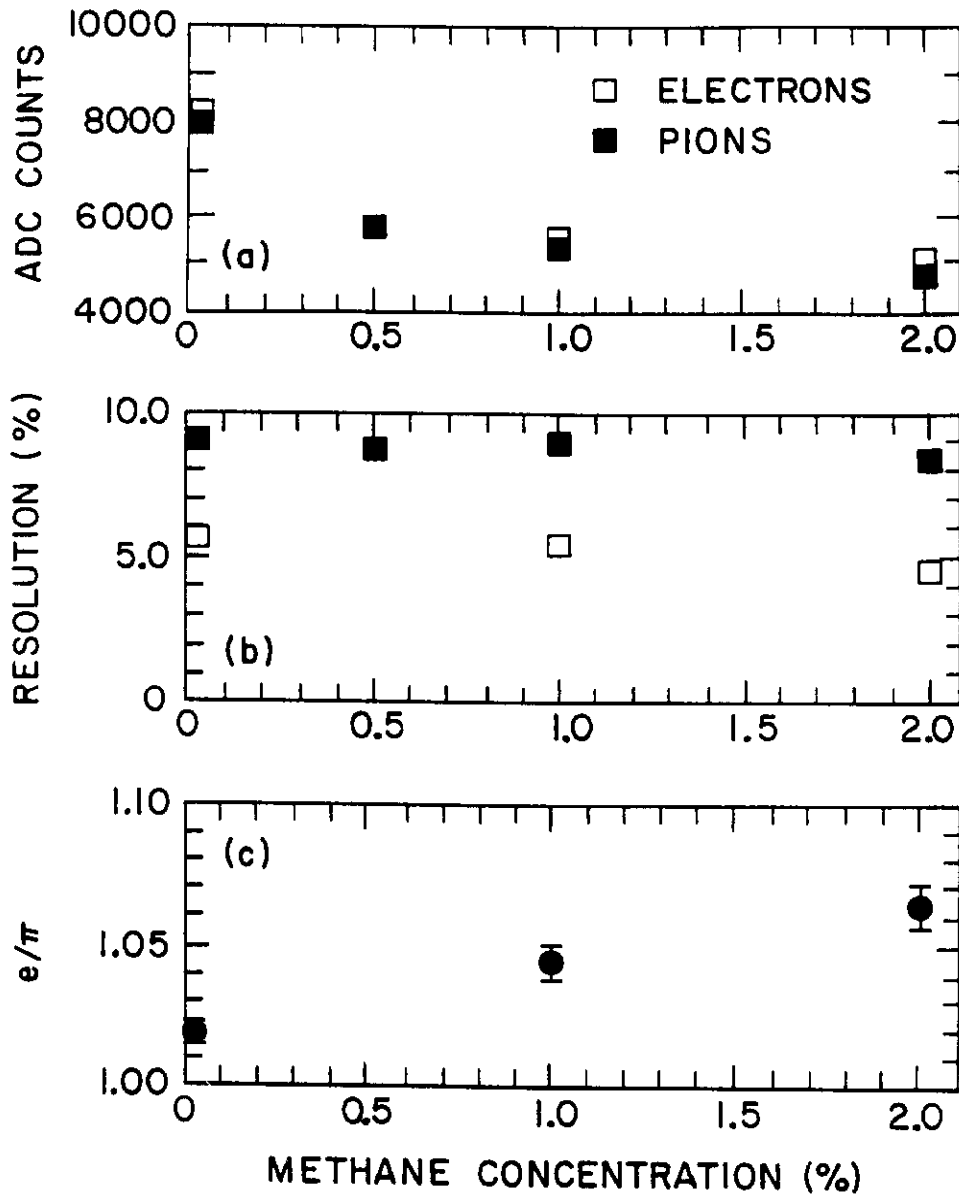


**Figure 10**

Effects of adding small amounts of methane to the liquid argon in the ECMH module. Methane concentration is in molar percent.

The incident particles were 50 GeV pions and electrons. The plots show (a) the response in ADC counts to electrons and pions, (b) the resolution ( $\sigma/\mu$ ), and (c)  $e/\pi$  after corrections (errors are statistical only).